URSI GASS 2020, Rome, Italy, 29 August - 5 September 2020

Propagation characteristics of whistler mode chorus in the outer radiation belt deduced from the Arase observation

Satoshi Kurita* (1), Yoshizumi Miyoshi(1), Yoshiya Kasahara (2), Hirotsugu Kojima(3), Shoya Matsuda(4)), Ayako Matsuoka(4), and Iku Shinohara(4)
(1) Institute for Space-Earth Environmental Research, Nagoya University, Nagoya, Japan
(2) Graduate School of Natural Science and Technology, Kanazawa University, Kanazawa, Japan
(3) Research Institute for Sustainable Humanosphere, Kyoto University, Uji, Japan
(4) Institute for Space and Astronautical Science, Sagamihara, Japan

Abstract

We investigated propagation characteristics of both lower-band and upper-band chorus (LBC and UBC) observed by the Arase satellite using the data processed by Onboard Frequency Analyzer (OFA), which is one of the receivers of the Plasma Wave Experiment (PWE). OFA provides spectral matrices of wave magnetic and electric fields separately. The magnetic spectral matrices were used to estimate propagation parameters of LBC and UBC. We derived occurrence frequency distributions of wave vector direction and wave power of these waves as a function of magnetic latitudes. We show that LBC and UBC can be categorized into several groups in terms of their wave vector directions and wave power. This categorization gives new insights and questions on the generation and propagation of LBC and UBC.

1 Introduction

The wave-particle interactions play crucial roles in the dynamics of Earth's inner magnetosphere. In particular, the dynamic variations of radiation belt electrons have been considered as the result of acceleration and loss of energetic electrons through interaction between electrons and various types of plasma waves [1]. It has been suggested that whistler mode chorus significantly contributes to both acceleration and loss of radiation belt electrons via wave-particle interactions [2].

It is important to understand the properties of whistler mode chorus. In particular, an important feature of chorus is its propagation characteristics, which have been mainly investigated by using the ray tracing technique [3]. Recently the propagation characteristics of chorus waves have been investigated [4], while the observations are limited near the equator. Data from the Cluster satellites enables to examine properties of chorus in the wide magnetic latitude (MLAT) range. It is found that intense lower-band chorus (LBC, typical frequency range between 0.1-0.5 f_{ce0}, where f_{ce0} is the equatorial gyrofrequency) can propagate up to 40 degrees with the wave vector directions parallel to the local magnetic field [5]. This propagation characteristics are not explained by the canonical ray tracing studies since the ray tracing predicts that the wave vector direction of chorus rapidly deviates from the local magnetic field during its propagation.

None of the satellite missions except ERG/Arase can verify the propagation of LBC shown by the Cluster measurements since the Arase satellite has a unique orbit which covers MLAT range from the equator up to 50 degrees. This paper aims to derive the propagation characteristics of both LBC and upper-band chorus (UBC, typical frequency range between 0.5-0.8 f_{ce0}). The propagation characteristics of UBC have not been studied by using the Cluster measurements.

2 Specification of PWE/OFA onboard Arase and Wave Propagation Analysis

The PWE [6] consists of two pairs of wire probe antennas (WPT) [7], tri-axial magnetic search coils (MSC) [8], and receivers which cover three different frequency range. WaveForm Capture/Onboard Frequency Analyzer (WFC/OFA) [9] processes signal from WPT and MSC in the frequency range from a few Hz to 20 kHz. OFA provides not only power spectra of electric and magnetic fields (OFA-SPEC) but also spectral matrices of electric and magnetic fields (OFA-MATRIX). OFA-MATRIX is generated with a time cadence eight times larger than the generation time interval of OFA-SPEC. OFA has been nominally operated to provide OFA-SPEC every 1 second. Thus OFA-MATRIX is provided every 8 seconds.

We have evaluated the propagation parameters of whistler mode chorus using OFA-MATRIX. The singular value decomposition (SVD) technique [10] is applied to spectral matrices of magnetic fields. The wave vector directions, ellipticities, and planarity estimators are obtained from the method.

3 Statistical Investigation of propagation characteristics of LBC and UBC

3.1 Analysis method

We statistically derived the MLAT distributions of wave vector direction and wave power of magnetic fields of both LBC and UBC using the data obtained by PWE/OFA from

the end of March 2017 to April 2019. We focused our analysis on the waves observed in the magnetic local time (MLT) range between 0 and 9, and the L* range between 3.5 and 6.0, where L* is the Roederer L evaluated using the TS04 magnetic field model [11]. The equatorial gyrofrequency f_{ce0} is evaluated as $f_{ce0} = f_{ceM}\ B_0/B_M$, where f_{ceM} is the equatorial gyrofrequency from the TS04 model, B_0 is the magnetic field intensity at the satellite location, and B_M is the local magnetic field intensity from the TS04 model. LBC and UBC are defined as the waves in the frequency range of 0.1-0.5 f_{ce0} and 0.5-1 f_{ce0}, respectively. The inaccuracy of f_{ce0} would result in contamination of the properties of LBC into those of UBC, and vice visa. To exclude noises and unnatural signals, we defined the threshold values for the ellipticity and the planarity. Since whistler mode waves are right-handed polarized, the ellipticity value of 0.2 is chosen to exclude linearly and left-handed polarized waves. The planarity value of 0.8 is selected to ensure that the estimated wave vector direction is reliable. We use a ratio of the magnetic field intensity at the satellite location to the equatorial magnetic field intensity as a proxy of MLAT. The ratio is mapped onto the dipole magnetic field model to obtain MLAT in the dipole magnetic field model.

3.2 Latitudinal Distribution of Wave Normal Angle of LBC and UBC

Figure 1a shows the occurrence frequency distribution of the wave normal angle of LBC as a function of MLAT. The occurrence frequency is computed if a bin contains the number of samples above 10. The occurrence frequency is normalized in each MLAT interval. It is found that LBC with the wave vector direction parallel to the local magnetic field is observed from the equator to 40 degrees. LBC with highly oblique wave normal angles appear near the equator to 30 degrees, and the wave normal angle gradually increases as MLAT is higher. The distribution shows that waves with wave normal angles very close to zero are less frequently observed compared to waves slightly oblique wave normal angles (5-15 degrees), which is caused by the fact that a solid angle is getting smaller in a smaller wave normal angle interval. This effect can be corrected by Jacobian $\sin\theta$, which is used to the transformation between spherical and Cartesian coordinate systems. The corrected occurrence frequency of the wave normal angle is shown in Figure 1b. It is found that LBC with the wave normal angle close to zero dominantly appears from the equator to higher latitudes. The fraction of highly oblique LBC is below 10 % of LBC with the parallel wave vector at all latitude intervals.

Figure 2a shows the occurrence frequency distribution of the wave normal angle of UBC as a function of MLAT. Similar to Figure 1a, the occurrence frequency is normalized at each latitude interval. UBC with wave vector directions parallel to the local magnetic field is observed from the equator to ~5 degrees, then appears again at higher latitude range from 25 to 40 degrees. Highly oblique LBC appears from the equator to 30 degrees, and the wave normal angle gradually increases as the MLAT is higher.

Figure 2b shows the occurrence frequency of the wave normal angle after the correction of the solid angle effect. UBC with parallel wave vector is dominant in the MLAT range of 0-5 degrees, then the occurrence of highly oblique UBC is comparable to that of UBC with the parallel wave vector in the MLAT range of 5-25 degrees. Parallel propagating UBC is dominant again in the MLAT above 25 degrees. However, it is speculated that there is the contamination of LBC information into the UBC frequency range at high latitudes since it is difficult to explain re-appearance of UBC with parallel wave vector at high latitudes. This issue is discussed in the latter section.

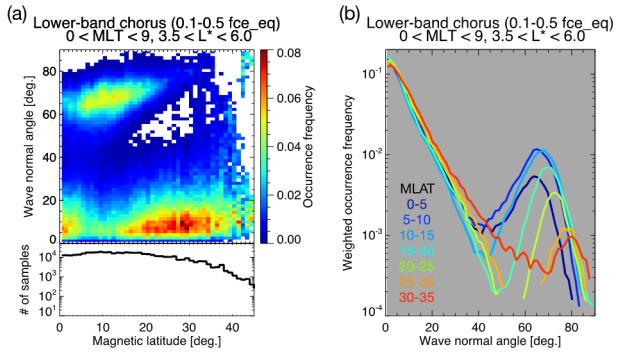

Figure 1. (a) Occurrence frequency distribution of wave normal angle of LBC as a function of MLAT. The number of spectra at each latitude interval is shown on the bottom. **(b)** Occurrence frequency distribution of wave normal angle of LBC corrected for effect on the small solid angle in the small wave normal angle intervals.

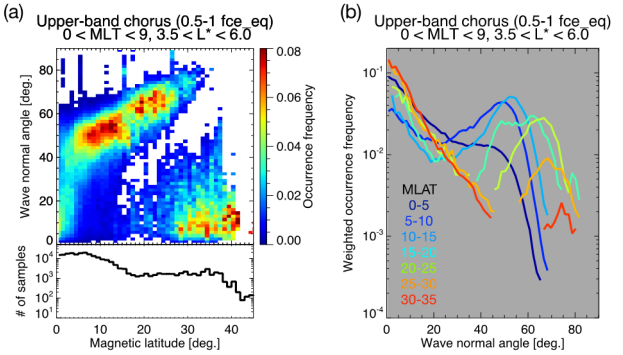

Figure 2. (a) Occurrence frequency distribution of wave normal angle of UBC as a function of MLAT. The number of spectra at each latitude interval is shown on the bottom. **(b)** Occurrence frequency distribution of wave normal angle of UBC corrected for effect on the small solid angle in the small wave normal angle intervals.

3.3 Latitudinal Distribution of Wave Power of LBC and UBC

Figures 3a and 3b show the occurrence frequency distributions of wave power of LBC and UBC as a function of MLAT, respectively. These waves have the wave

normal angle below 30 degrees, and the wave power is computed by integrating over the frequency range of LBC and UBC. The occurrence frequency is calculated if a bin contains the number of samples above 4. The occurrence frequency is normalized at each latitude interval.

LBC has wave power ranging from 1 pT^2 to 1000 pT^2 from the equator to high latitudes. Large amplitude LBC with wave power greater than 1000 pT^2 is most frequently observed near the magnetic equator, and the occurrence of the large amplitude waves decreases as MLAT increases. UBC with parallel wave vector has wave power ranging from 1 to 10000 pT^2 , and the wave power significantly decreases in the MLAT above 10 degrees. Waves with wave power ranging from 1 to 1000 pT^2 appear again in MLAT above 25 degrees. The wave power range is similar to that of LBC in the same MLAT range.

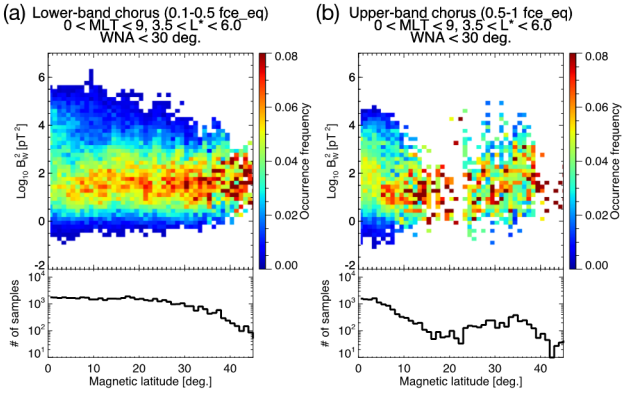

Figure 3. (a) Occurrence frequency distribution of wave power of LBC as a function of MLAT. The number of samples at each latitude interval is shown on the bottom. **(b)** Similar plot for Figure 3a except wave power of UBC. Both LBC and UBC have wave normal angles below 30 degrees.

Figures 4a and 4b show the occurrence frequency distribution of wave power of highly oblique LBC and UBC as a function of MLAT, respectively. We used the threshold of the oblique wave normal angle of LBC and UBC as 55 and 35 degrees, respectively. The wave power is computed by integrating over the frequency range of highly oblique LBC and UBC. Similar to Figure3, the occurrence frequency is calculated if a bin contains the number of samples above 4. The occurrence frequency is normalized at each latitude interval. The wave power of the highly oblique LBC is observed to lie between 1pT^2 and 100 pT^2 near the magnetic equator, while the fraction of the large amplitude waves increases as the MLAT increases. The wave power in the MLAT from 10 to 20 degrees ranges from 1 pT^2 up to 10000 pT^2. Similar tendency is seen in the occurrence distribution of wave power of highly oblique UBC. The fraction of large amplitude and oblique UBC increases from the equator to 10 degrees, then the large amplitude UBC less frequently observed as the MLAT increases up to 20 degrees.

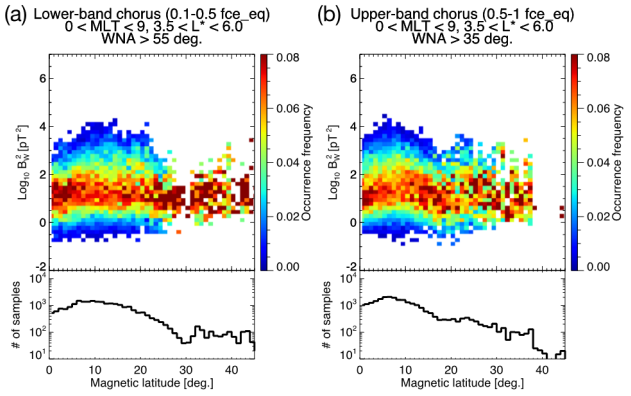

Figure 4. (a) Occurrence frequency distribution of wave power of LBC as a function of MLAT. The number of samples at each latitude interval is shown on the bottom. **(b)** Similar plot for Figure 3a except wave power of UBC. LBC and UBC have wave normal angles above 55 and 35 degrees, respectively.

4. Discussion and Summary

The statistical analysis of the propagation characteristics of LBC and UBC based on the two-year Arase observation shows systematic propagation patterns of both LBC and UBC. Firstly, the Arase observation verifies the Cluster finding that the majority of LBC propagates up to 40 degrees with the wave vector close to the local magnetic field. The wave power distribution of LBC with parallel wave vector shows that the large amplitude LBC appears only near the magnetic equator, although the majority of LBC propagates up to 40 degrees in a statistical sense. One explanation of the confinement of the large amplitude LBC near the equator is that these waves propagate unducted mode, and the wave power decreases due to Landau damping during its propagation [3]. Another possibility is the nonlinear aspect of wave-particle interactions. Large amplitude waves can resonantly accelerate electrons in a short time interval through nonlinear wave-particle interactions [12]. This acceleration process results in damping of wave power, which may explain the decrease in the occurrence frequency of the large amplitude waves at high latitudes.

The Arase observation newly reveals the wave normal angle of UBC in the wide MLAT range. It is found that UBC with wave vector direction close to the local magnetic field is observed only near the equator. The highly oblique UBC is dominantly observed in the MLAT from 5 to 25 degrees. UBC with parallel wave vector appears again in high latitudes. We have visually inspected the events which contribute to the events categorized into UBC with parallel wave vector at high latitudes. It is found that, in many cases, f_{ce0} lies on a single band chorus, which results in the categorization of the single band wave into LBC and UBC. We speculate that the UBC events with parallel wave vector observed at high latitudes are an artifact that is caused by inaccurate estimation of the equatorial gyrofrequency. This speculation could be supported by the fact that the wave power of UBC with parallel wave vector

is not continuously distributed but split into the two MLAT ranges.

The highly oblique LBC and LBC are observed to propagate unducted mode since the wave normal angle of the waves increases from the equator to high latitudes, as predicted by the canonical ray tracing studies. Based on the calculation of linear grow rates, highly oblique waves are strongly damped by Landau damping [13]. On the other hand, the Arase observation suggests that the highly oblique LBC and UBC propagates above 20 degrees. The wave power distributions of highly oblique LBC and UBC imply that the amplitude of these waves increases during their propagation since the fraction of large amplitude waves tends to increases as MLAT increases. This propagation characteristics is still an open issue.

Based on the ray tracing study, the propagation of LBC with parallel wave vector to high latitudes can be explained if there are density enhancement in the magnetosphere [14]. Even though the size of density enhancement is small, and they are localized, LBC can be guided by the density enhancements [14]. Considering that a region between density enhancements can be a localized density depletion, UBC with parallel wave vector can be guided in the density depletion [15], which results in propagation of UBC to high latitudes. However, the Arase observation does not support this idea. The explanation for the different propagation characteristics between LBC and UBC needs to be addressed in cooperation between theory and observation, which is left as our future works.

6 Acknowledgements

This study has been supported by Grant-in-Aid for Scientific Research (15H05815, 15H05747, 16H06286, 16H04056, 17H06140). This study was also supported by JSPS Bilateral Open Partnership Joint Research Projects.

7 References

1. Thorne, R. M. (2010), Radiation belt dynamics: The importance of wave-particle interactions, Geophys. Res. Lett., 37, L22107, doi:10.1029/2010GL044990.

2. Bortnik, J., & Thorne, R. M. (2007). The dual role of ELF/VLF chorus waves in the acceleration and precipitation of radiation belt electrons. Journal of Atmospheric and Solar-Terrestrial Physics , 69, 378-386.

3. Chen, L., R. M., Thorne, W., Li, and J., Bortnik (2013), Modeling the wave normal distribution of chorus waves, J. Geophys. Res. Space Physics, 118, 1074-1088, doi:10.1029/2012JA018343.

4. Li, W., Santolik, O., Bortnik, J., Thorne, R. M., Kletzing, C. A., Kurth, W. S., and Hospodarsky, G. B. (2016), New chorus wave properties near the equator from Van Allen Probes wave observations, Geophys. Res. Lett., 43, 4725–4735, doi:10.1002/2016GL068780.

5. Santolík, O., Macúšová, E., Kolmašová, I., Cornilleau-Wehrlin, N., and de Conchy, Y. (2014), Propagation of lower-band whistler-mode waves in the outer Van Allen belt: Systematic analysis of 11 years of multi-component data from the Cluster spacecraft, Geophys. Res. Lett., 41, 2729– 2737, doi:10.1002/2014GL059815.

6. Y. Kasahara et al. (2018), The Plasma Wave Experiment (PWE) on board the Arase (ERG) satellite, Earth, Planets and Space, 10.1186/s40623-018-0842-4.

7. Kasaba, Y., et al. (2017), Wire Probe Antenna (WPT) and Electric Field Detector (EFD) of Plasma Wave Experiment (PWE) aboard the Arase satellite: specifications and initial evaluation results. Earth Planets Space 69, 174.

8. Ozaki, M., S. Yagitani, Y. Kasahara, H. Kojima, Y. Kasaba, A. Kumamoto, F. Tsuchiya, S. Matsuda, A. Matsuoka, T. Sasaki, and T. Yumoto (2018), Magnetic Search Coil (MSC) of Plasma Wave Experiment (PWE) aboard the Arase (ERG) satellite, Earth, Planets and Space, 10.1186/s40623-018-0837-1.

9. Matsuda, S., et al. (2018), Onboard Software of Plasma Wave Experiment aboard Arase: Instrument Management and Signal Processing of Waveform Capture/Onboard Frequency Analyzer, Earth, Planets and Space, 10.1186/s40623-018-0838-0.

10. Santolík, O., M. Parrot, and F. Lefeuvre (2003), Singular value decomposition methods for wave propagation analysis, Radio Sci., 38, 1010, doi: 10.1029/2000RS002523, 1.

11. Tsyganenko, N. A., and Sitnov, M. I. (2005), Modeling the dynamics of the inner magnetosphere during strong geomagnetic storms, J. Geophys. Res., 110, A03208, doi:10.1029/2004JA010798.

12. Omura, Y., and D. Summers (2006), Dynamics of high-energy electrons interacting with whistler mode chorus emissions in the magnetosphere, J. Geophys. Res., 111, A09222, doi:10.1029/2006JA011600.

13. Kennel, C. F., & Thorne, R. M. (1967). Unstable growth of unducted whistlers propagating at an angle to the geomagnetic field. Journal of Geophysical Research, 72 (3), 871–878.

14. Hanzelka, M., & Santolik, O. (2019). Effects of ducting on whistler mode chorus or exohiss in the outer radiation belt. Geophysical Research Letters, 46, 5735– 5745. https://doi.org/10.1029/2019GL083115.

15. Smith, R. L., Helliwell, R. A., and Yabroff, I. W. (1960), A theory of trapping of whistlers in field-aligned columns of enhanced ionization, J. Geophys. Res., 65(3), 815– 823, doi:10.1029/JZ065i003p00815.